Chapter V

CHAPTER V

SYNTHESIS, CRYSTAL GROWTH, AND STRUCTURAL DETERMINATION OF GUANIDINIUM-2-NAPHTHOATE ADDUCT

5.1 INTRODUCTION

An adduct is the formation of the direct addition of two or more distinct molecules resulting in a single reaction product that contains all atoms of the component with the formation of two chemical bonds and a net reduction in bond multiplicity in at least one of the reactants [1]. Otherwise, it is defined as a combined unit of acid and base moiety at ambient conditions composed of hydrogen bonds in the crystalline form Intermolecular hydrogen bonding plays a leading role in the stabilization of adducts [2]. In this chapter, a new kind of acid adduct formed by the reaction of guanidium with a 2-naphthoic acid crystalline form was discussed. The crystal was characterized by single-crystal XRD, and FT-IR spectroscopy, and their thermal behavior has also been analyzed by simultaneous TG-DTA [3].

5.2 EXPERIMENT

5.2.1 Preparation of acid adduct

Naphthoic acid has extremely low solubility, so it is very hard to grow a single crystal. We adopted many methods for single crystals and finally, we grew a single crystal by slow evaporation method with 2-naphthoic acid - guanidine in a 1:1 water-alcohol medium. They were stirred to obtain a homogenous solution at pH 7 and the resulting solution was concentrated to a partial solution in a thermostatic water bath at 100 °C, and then it was kept in a dark room for the slow evaporation of the solvent. A colorless, rectangle-shaped crystal was obtained from the mother liquid after 15 days. The single crystal obtained was washed and filtered with an alcoholic solution to remove additional impurities. The synthesized crystal is shown in **Figure 5.1.**

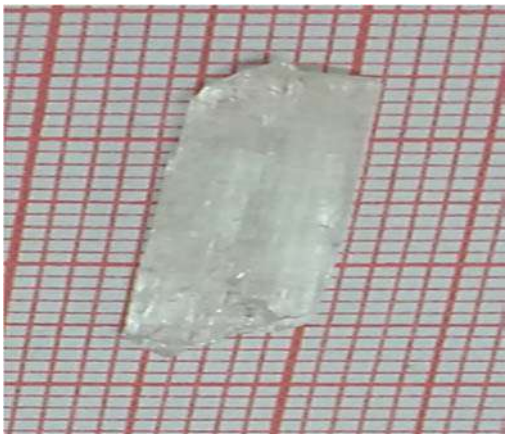

Figure 5.1 *Image of Guanidinium- 2- naphthoate crystal*

5.3 RESULT AND DISCUSSION

5.3.1 Crystal structure

The single crystal structure of the adduct is examined in **Figure 5.2 a**. The space group of the crystal is monoclinic and possesses P12 1/c 1 symmetry. The crystallographic data are detailed in **Table 5.1**. The bond distance and bond angle between the atoms were discussed in **Tables 5.2 and 5.3**. **Figure 5.2 b** represents the ORTEP crystal packing, and the molecular formula obtained is $C_{12}H_{13}N_3O_2^+$. The acid and the anions are linked through the hydrogen bond, in which they are represented by N-H…. O, and **Figure 5.2 c** examines the short contacts of the crystal. The zig-zag arrangement and the space-filling image are also shown in **Figure 5.3 (a-e).**

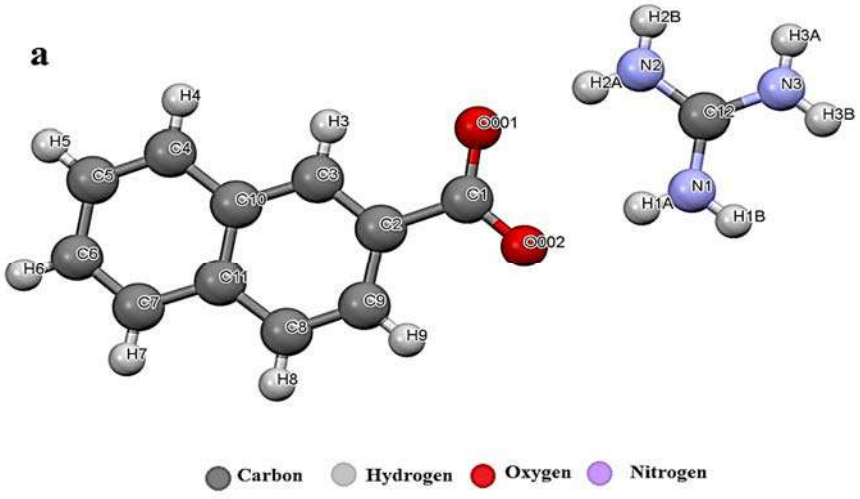

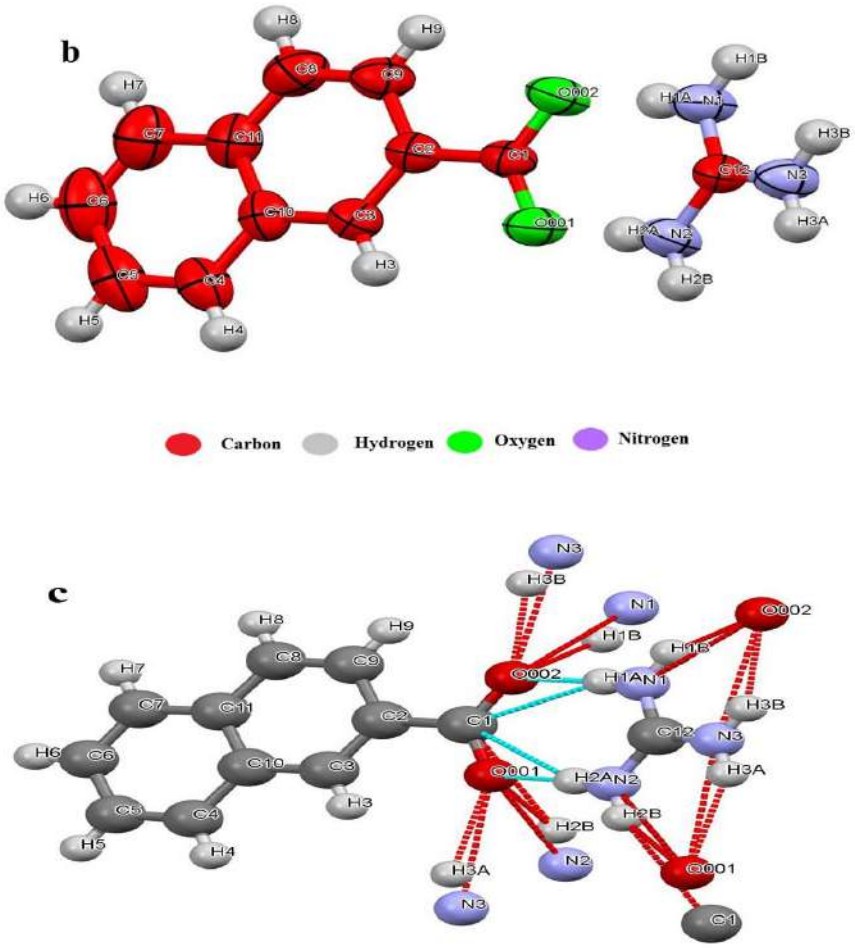

Figure 5.2 *a) Single crystal structure of the acid adduct (b) ORTEP diagram (c) Short contacts of the acid adduct.*

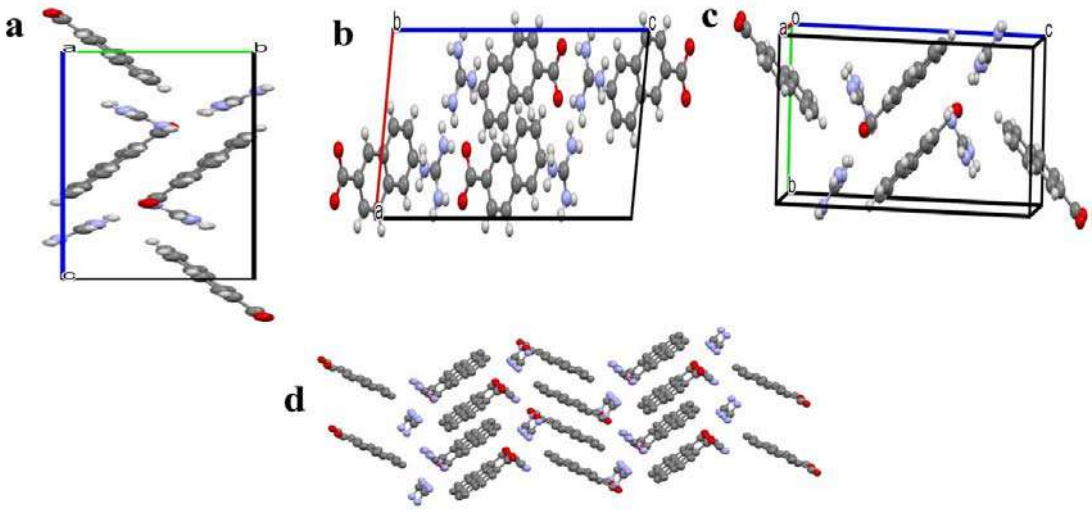

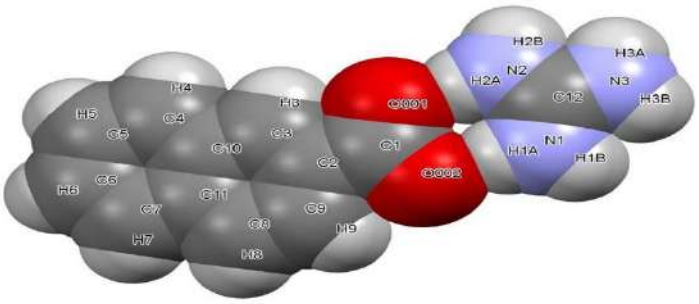

Figure 5.3 *Crystal observed along (a) 'a' axis, (b) 'b' axis, (c) 'c' axis direction, (d) Zig-Zag arrangement, and e) space-filling model.*

Table 5.1 *Crystallographic information of acid adduct.*	
Compound name	Guanidium- 2-naphthoate
Empirical formula	C_{12} H_{13} N_3 O_2
Molecular Weight	231.25
Temperature	273K
Wavelength	0.71073
Crystal system	Monoclinic
Space group	P 1 21/c 1
Hall Group	-P 2ybc
Cell lengths (Å)	**a** .0765(7) **b** 7.9306(7)**c** 9.3188(16)
Cell angles (°)	**α** 90 **β** 99.442(3)**γ** 90
Cell Volume ($Å^3$)	1220.63(18)
Z, Z'	**Z**: 4 **Z'**: 0
Absorption coefficient (mm^{-1})	0.088
R- factor (%)	4.22
hkl max	9, 9, 22
F000	488.0
F000'	488.21

Table 5.2 *Bond distance of the acid adduct.*			
Atom1	**Atom2**	**Cyclicity**	**Length**
O001	C1	acyclic	1.254(2)
O002	C1	acyclic	1.252(2)
C1	C2	acyclic	1.504(2)
C2	C3	cyclic	1.366(2)
C2	C9	cyclic	1.410(2)
C3	H3	acyclic	0.93
C3	C10	cyclic	1.413(2)
C9	H9	acyclic	0.93
C9	C8	cyclic	1.358(2)
C10	C4	cyclic	1.414(2)
C10	C11	cyclic	1.415(2)
C4	H4	acyclic	0.93
C4	C5	cyclic	1.360(2)
C11	C8	cyclic	1.411(2)
C11	C7	cyclic	1.416(2)
C8	H8	acyclic	0.93
C5	H5	acyclic	0.93
C5	C6	cyclic	1.395(4)
C7	H7	acyclic	0.93
C7	C6	cyclic	1.354(4)
C6	H6	acyclic	0.93
N3	H3A	acyclic	0.86
N3	H3B	acyclic	0.86
N3	C12	acyclic	1.322(2)
N2	H2A	acyclic	0.86
N2	H2B	acyclic	0.86
N2	C12	acyclic	1.313(2)
N1	H1A	acyclic	0.86
N1	H1B	acyclic	0.86
N1	C12	acyclic	1.315(2)

Table 5.3 *Bond angle of the acid adduct.*

Atom1	Atom2	Atom3	Angle
O001	C1	O002	123.1(1)
O001	C1	C2	118.3(1)
O002	C1	C2	118.6(1)
C1	C2	C3	120.4(1)
C1	C2	C9	120.7(1)
C3	C2	C9	118.9(1)
C2	C3	H3	119
C2	C3	C10	122.0(1)
H3	C3	C10	119
C2	C9	H9	119.7
C2	C9	C8	120.6(1)
H9	C9	C8	119.7
C3	C10	C4	122.3(1)
C3	C10	C11	118.7(1)
C4	C10	C11	119.0(1)
C10	C4	H4	119.7
C10	C4	C5	120.6(2)
H4	C4	C5	119.7
C10	C11	C8	118.3(1)
C10	C11	C7	118.5(1)
C8	C11	C7	123.3(2)
C9	C8	C11	121.7(2)
C9	C8	H8	119.2

Atom1	Atom2	Atom3	Angle
C11	C8	H8	119.2
C4	C5	H5	119.8
C4	C5	C6	120.4(2)
H5	C5	C6	119.8
C11	C7	H7	119.6
C11	C7	C6	120.8(2)
H7	C7	C6	119.6
C5	C6	C7	120.8(2)
C5	C6	H6	119.6
C7	C6	H6	119.6
H3A	N3	H3B	120
H3A	N3	C12	120
H3B	N3	C12	120
H2A	N2	H2B	120
H2A	N2	C12	120
H2B	N2	C12	120
H1A	N1	H1B	120
H1A	N1	C12	120
H1B	N1	C12	120
N3	C12	N2	120.0(1)
N3	C12	N1	120.1(1)
N2	C12	N1	119.8(1)

5.3.2 *Theoretical crystal morphologies*

The single crystal was projected in WinXmorph software to study the crystal morphology, as shown in **Figure 5.4a**. It exhibits the eight sets of facets such as (0,0,1), (0,0,-1), (0,1,0), (0,-1,0), (1,0,0), (-1,0,0), (1,0,-1) and (-1,0,1) in which (0,0,1) and (-1,0,1) represents the large facets. The angle between the plane represents the grown crystal morphologies as [0,0,1) & (0,0,-1)], [(0,0,-1) & (0,1,0)],[(0,1,0) & (0,-1,0)],[(0,-1,0) & (1,0,0)],[(1,0,0) & (-1,0,0)],[(-1,0,0) & (1,0,-1)], [(-1,0,0) & (1,0,-1) and [(-1,0,1) & (0,0,1)] is 35.26 °, 90 °, 0 °, 90 °,45°, 45°,90 ° respectively. **Figure 5.4b** is a stereographic projection used in crystallography and structural geology to describe the angular relationships among the crystal faces and geologic structures, respectively. The geodesic distance between the planes is denoted in dotted line [4].

The arrangement of the chromophore is indicated by the acute angle, which exhibits the plane 'a axis in **Figure 5.4c**. The plane group is vertical to its cation molecular units. The axis 'a' denotes a 13.75° angle [5]. The crystallographic deposit, CCDC number is 2196146.

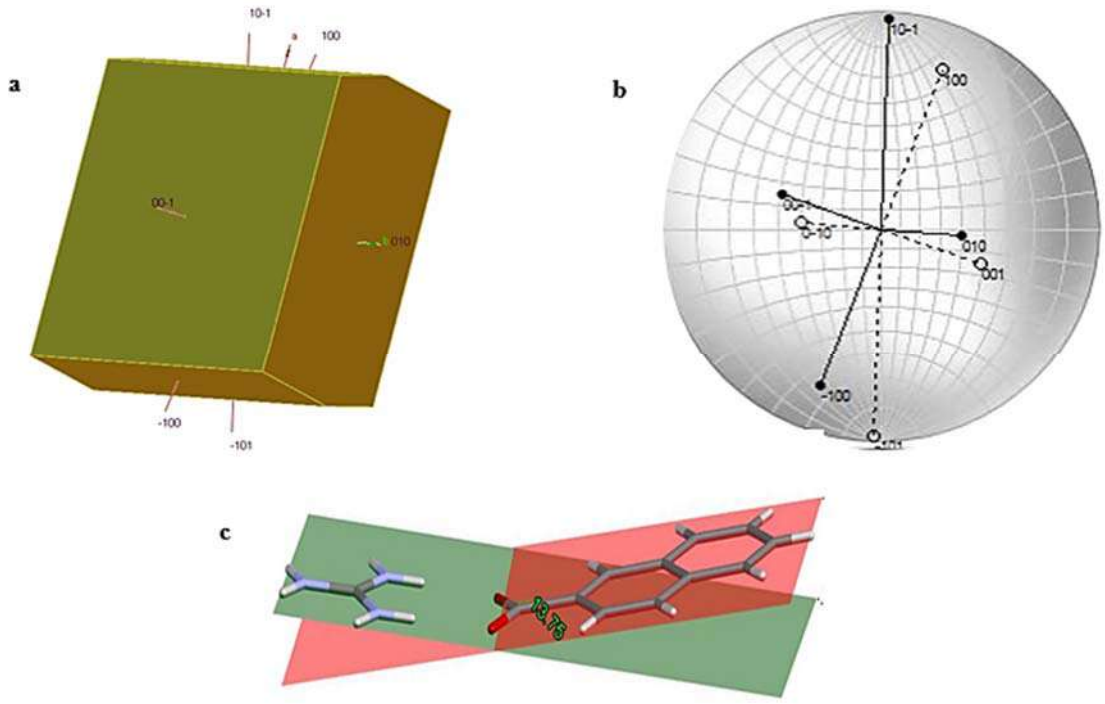

Figure 5.4 *(a) Morphology of the acid adduct (b) Stereographic projection, (c) Acute angle along the plane 'a' axis.*

5.3.3 FT-IR spectra

In the IR spectra of the acid adduct **(Figure 5.5)**, the -OH group displacement from 3505 cm^{-1} to 3605 cm^{-1} when compared with free acid is due to the H bonding interaction. The symmetric and asymmetric bands of carboxylate groups range from 1578-1557 cm^{-1} and 1379-1352 cm^{-1} respectively. The broad band around the region 3195-3300 cm^{-1} is due to N-H frequency. The peak at 1217-1352 cm^{-1} refers to the C-N stretching frequency where ɣ (C= N) band of guanidine was shifted to the lower wavenumber which confirmed the formation of the adduct [6].

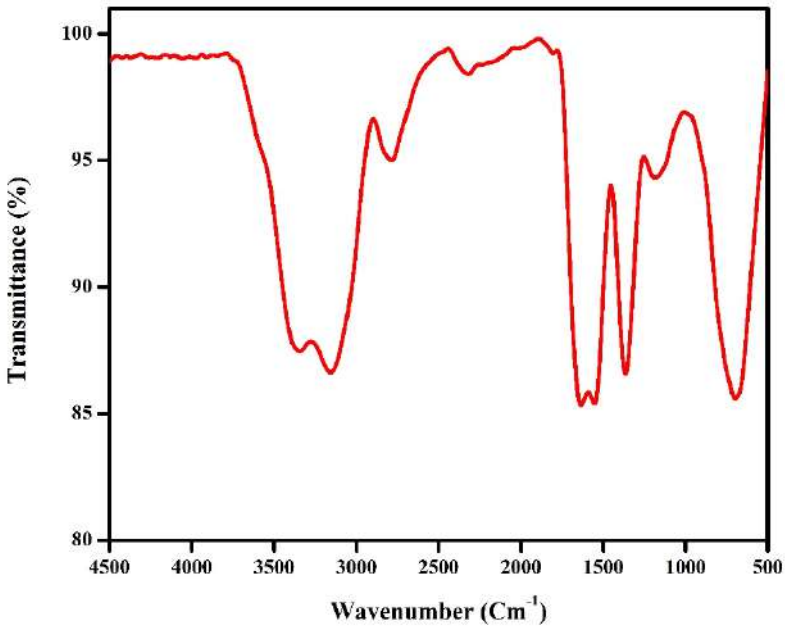

Figure 5.5 *FT-IR of acid adduct*

5.3.4 UV-visible spectra

The optical properties of the adduct were illustrated from UV-visible spectroscopy (**Figure 5.7a)**, which was recorded from 200-800 nm. The peak at 230 nm is due to $\pi \rightarrow \pi$ transition and implies the presence of the unsaturated group in the adduct. Above 450 nm, there is a peak due to the $n \rightarrow \pi$ transition.

The absorption coefficient, refractive index, extinction coefficient, and skin depth were determined by Tauc's plot. The absorption coefficient wavelength was determined by using the following equation **Eq. (5.1)**.

$$\alpha = \frac{2.303\ A}{t}$$ **Eq. (5.1)**

The suitable wavelength penetrated by the sample was determined before absorption. The plot was drawn against the absorption coefficient vs. energy band (Eg) as shown in **Figure 5.7b** and the fundamental absorption was noticed at 4.7 e V. **Figure 5.7c** represents Tauc's plot, and the band energy gap was determined by $\alpha h\nu = A(h\nu\text{-}Eg)^2$ where Eg values are 4.6 eV which represent semiconductor nature. **Figure 5.7d** shows the refractive index plot of the adduct, and was calculated by using the equation, $n = \{(1/T) + (1/(T\text{-}1)\}^{1/2}$ in which the higher refractive indexes were detected at 234 nm and lower wavelengths are due to the effect of fundamental absorption. **Figure 5.7e** shows the extinction coefficient plot calculated using the equation, $k = \alpha\lambda/4\pi$. The plot substantiates that photon energy increases while the extinction coefficient increases, and then after 200 nm they are gradually reduced. **Figure 5.7f** displays the skin depth of the sample, ($\delta = 1/\alpha$) and shows the increase in photon energy decreases the skin depth value [7,8,9].

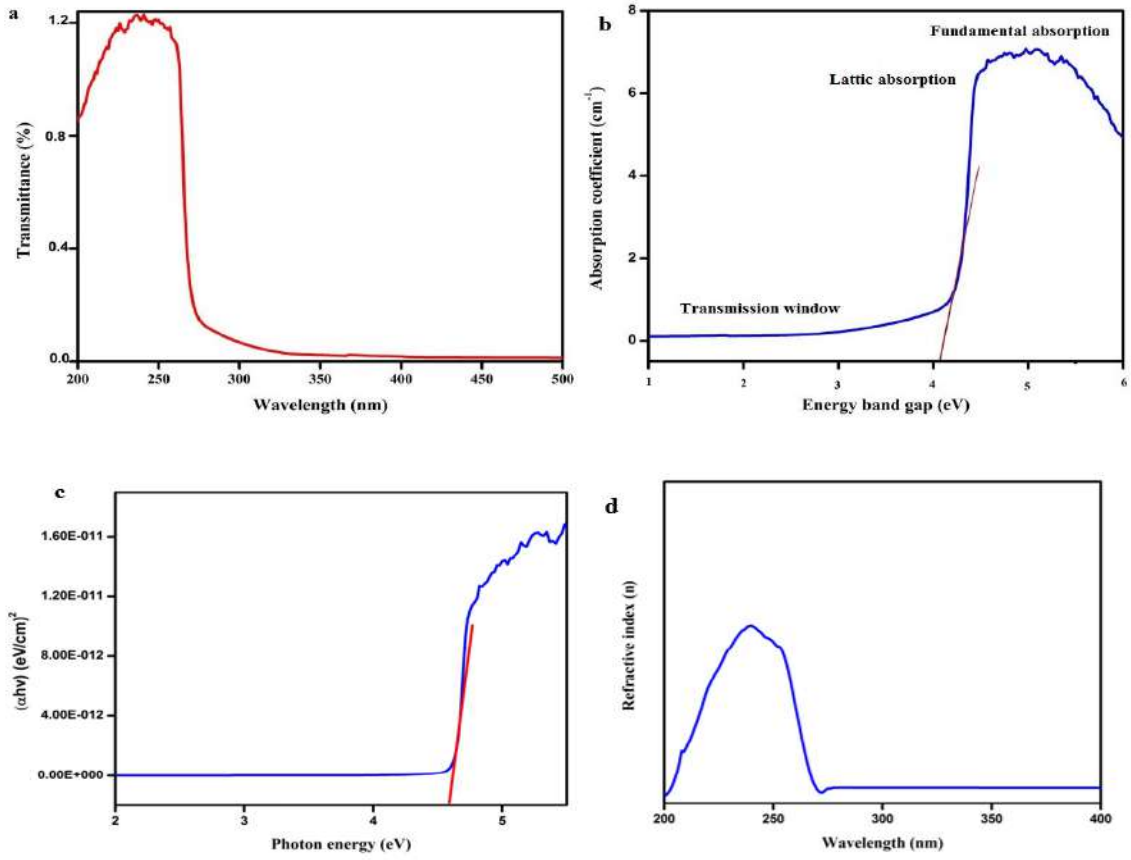

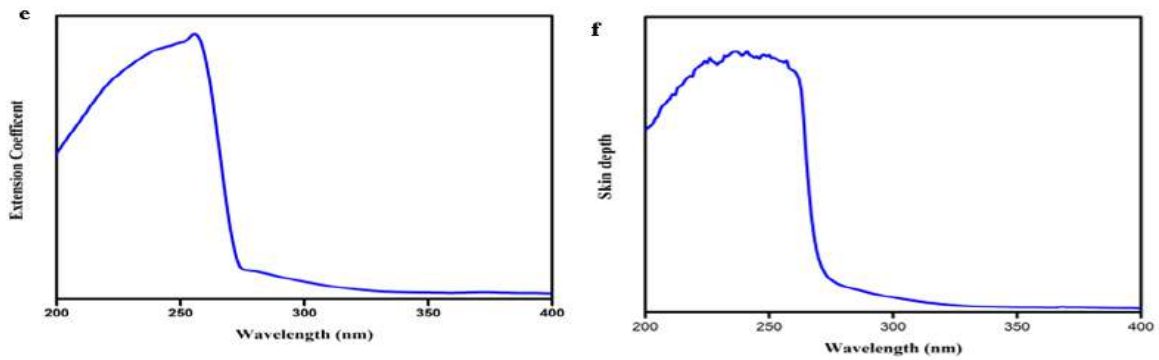

Figure 5.7 *(a) UV spectra, (b) Absorption coefficient, (c) Tauc's plot, (d) Refractive index, (e) Extinction coefficient, and (f) Skin Depth of the adduct*

5.3.5 Thermal analysis

The thermal analysis of the adduct was performed from 0 to 600 °C at nitrogen atmosphere. **Figure 5.8** represents the various phases of thermal decomposition. The first stage of decomposition is at 200 °C. The sharp endothermic peak occurred at 198 °C, and t 315 °C, is due to the removal of adsorbed moisture and melting of the crystal. At last, a final decomposition occurred above 399°C, resulting in the formation of carbon residue as the final product. The thermogram data confirms the thermal stability of the crystal.

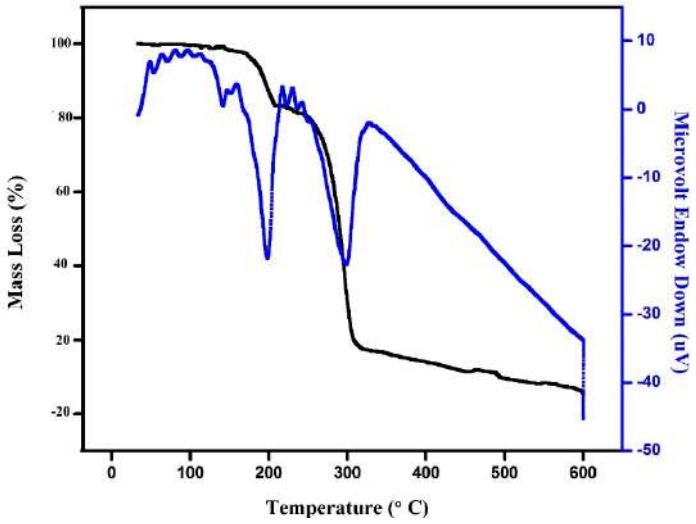

Figure 5.8 *Thermal analysis of adduct.*

Thermodynamic parameters for the adduct were calculated using the Coats-Redfern equations,

$$\log_{10}\left[\frac{1-(1-\alpha)^{1-n}}{T^2\,(1-n)}\right] = \log_{10}\left[\frac{AR}{E\alpha}\right]\left[1-\frac{2RT}{E\alpha}\right] - \frac{E}{2.303\,RT} \qquad \textbf{Eq. (5.2)}$$

Where α, is the sample decomposed at a given time (t),

W_o is the initial weight,

W_f is the final weight,

W_t, the weight of the sample at any temperature.

T is an absolute temperature

A is the frequency factor

E is the activation energy and

R is gas constant

The plot was drawn against $\log_{10}\left[\frac{1-(1-\alpha)^{1-n}}{T^2\,(1-n)}\right]$Vs 1/T is displayed in **Figure 5.9**, at three different stages of temperature decomposition namely 298 K, 333K, and 543 K. The activation energies of E_a and slope values are tabulated in **Table 5.5**. By using the following equation the value of enthalpy, entropy, and Gibbs free energy [10,11] was calculated.

Entropy change, $\Delta S = R*\ln(Ah/kT)$ **Eq.(5.3)**

Enthalpy change, $\Delta H = E_a - RT$ **Eq. (5.4)**

Gibbs free energy $\Delta G = \Delta H - T\Delta S$ **Eq. (5.5)**

The negative value of ΔS represents that the reaction is slower and spontaneous. The positive ΔH specifies the reaction is an endothermic reaction in nature, and the positive ΔG value proves that products possess more free energy. The slope values were correlated with the linear fit in which the R^2 value produced was 0.88, 0.89, and 0.99 [12].

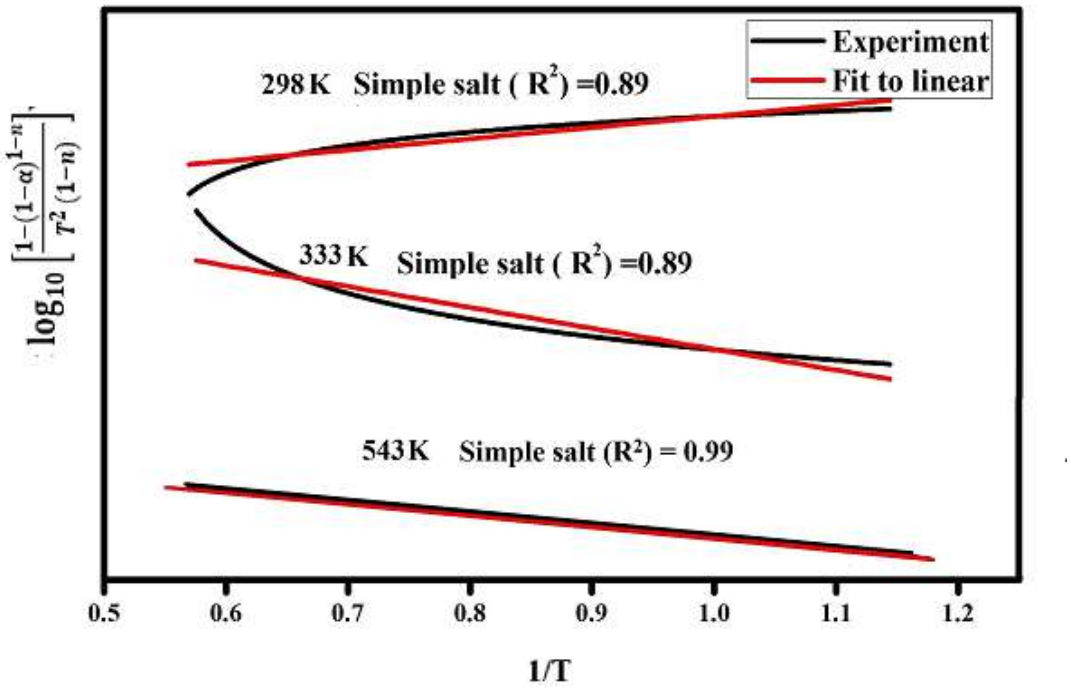

Figure 5.9 *Thermodynamic parameters at 298 K, 333K, and 543 K.*

Table 5.5 *Thermodynamic parameters.*

Temperature in K	Ea kJ/mol	ΔS JK^{-1}/mol	ΔH kJ/mol	ΔG kJ/mol
298	41.13	-26.43	28.43	12.08
333	41.13	-20.78	28.43	11.84
543	62.06	-15.21	23.27	11.53

5.3.6 Powder- XRD

The powder Xrd pattern of the adduct was measured at 2 Θ value ranging from 10 ° to 70°, and the wavelength ranged from λ= 1.54056 Å. The peak diffraction was detected, and the hkl values were studied. The peak found theoretically coincides with the XRD data, which confirms the synthesized adduct was highly crystalline, as indicated in **Figure 5.10 (a, b)**.

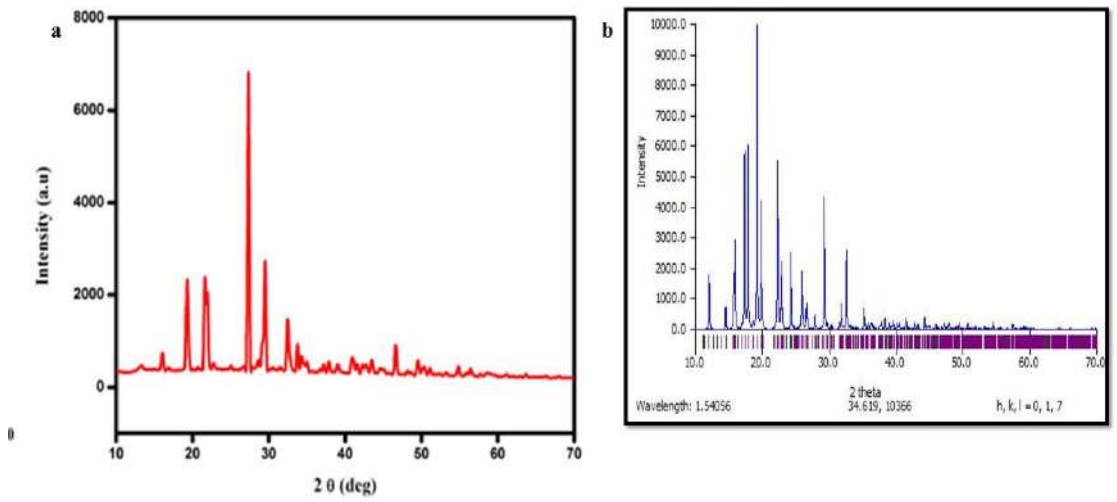

Figure 5.10 *Powdered-XRD (a) Experimental data (b) Theoretical method.*

5.4 COMPUTATIONAL STUDY FOR CRYSTAL

The atomic configuration of the ions was studied computationally using the Gaussian 09W software, and the stable geometry was obtained by optimizing using the DFT//B3LYP and their basic set with 6.31G(d, p) shown in **Figure 5.11a**.

Figure 5.11b demonstrates frontier molecular orbital (FMO), which signifies the chemical stability and interaction of the compounds on the active sites. The HOMO-LUMO implies charge transfer among the aromatic ring and the amino groups. The E_{HOMO} and E_{LUMO} were calculated at -11.814 eV and -4.5054 eV, respectively. The negative values demonstrate the stability of the sample and ΔE value was found to be 7.31 eV [13,14].

Chemical potential (μ), electro negativity (χ), chemical hardness (η), global softness (s), and electrophilicity (ω) were calculated from HOMO and LUMO, where HOMO intimates the ionization energy and LUMO describes the electron affinity of the adduct crystal.

$$\mu = -(IE+EA) / 2 \quad \textbf{Eq. (5.6)}$$

$$\chi = (IE+EA) / 2 \quad \textbf{Eq. (5.7)}$$

$$\eta = (IE-EA) / 2 \quad \textbf{Eq. (5.8)}$$

$$s = 1 / 2\eta \quad \textbf{Eq. (5.9)}$$

$$\omega = \mu^2 / 2\eta \quad \textbf{Eq. (5.10)}$$

The outcomes of global reactivity are listed in **Table 5.6**. ɳ and s indicate that Global softness (s) is less than chemical hardness (ɳ) and electrophilicity (ω) shows a higher value, which signifies the charges from the closer molecules.

The Molecular Electrostatic Potential surface denotes the interaction of the molecule, electron density, electrophilic, and nucleophilic (**Figure 5.11c).** The negative electrostatic potential is signified by red, and the positive electrostatic potential is represented by blue. They ranged from -0. 05a.u, which indicates the deep red color, to +0. 05a.u, which represents the deep blue color. The surface is mostly covered in white, which indicates it is non-polar.

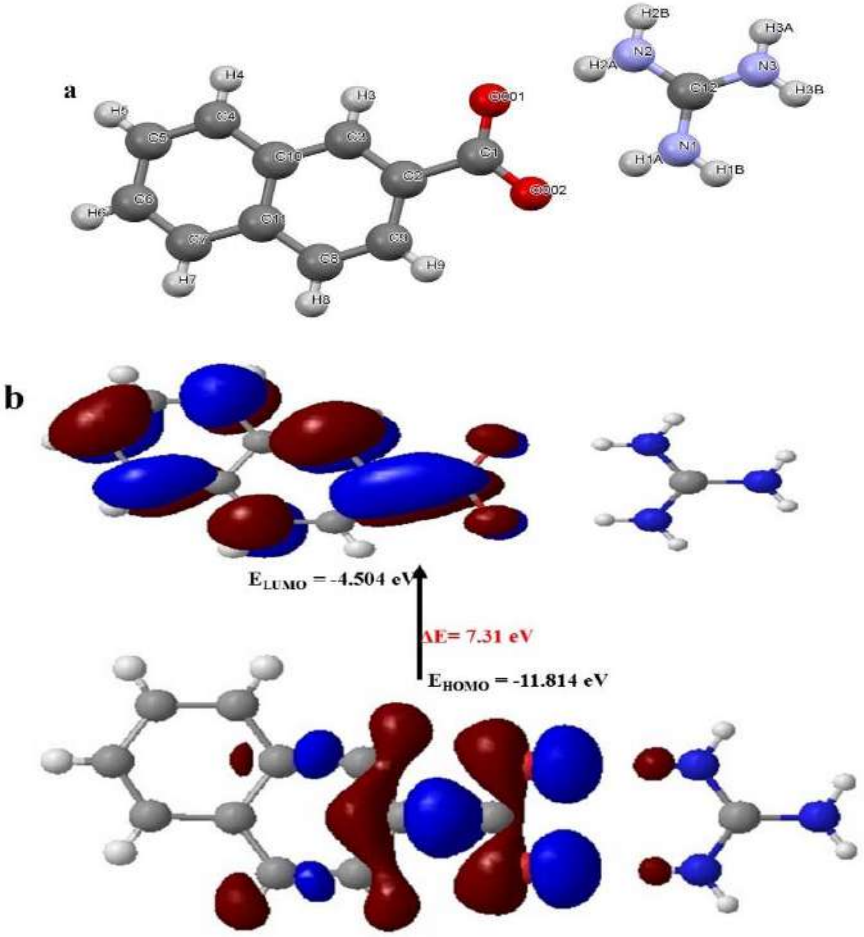

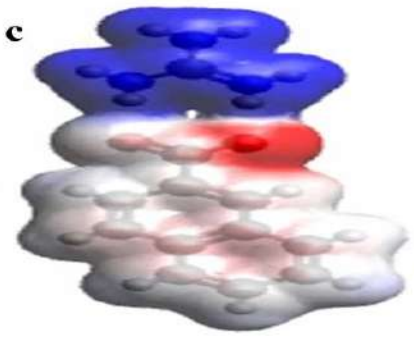

Figure 5.11 *(a) Orientation geometrical of the acid adduct, (b) HOMO and LUMO of the acid adduct, and (c) Electrostatic potential of the acid adduct.*

Table 5.6 *Global Reactivity Properties*	
Parameters	**Energy values (eV)**
Chemical potential (μ)	-16.318
Electronegativity (χ)	16.318
Chemical hardness (η)	3.655
Global softness (s)	1.8275
Electrophilicity (ω)	36.42

5.5 HIRSHFELD SURFACE ANALYSIS

Hirshfeld surface analysis **Figure 5.12a** shows the interaction of the atoms and their close contact in the crystal packing. It generates the $d_{norm,}$ in which two types of distance, di (internal) and de (external), range from -0.5324 (red) to 2.2206 (blue). In a 3D image, the red region shows the oxygen and the hot spot is described as a hydrogen bond with contact with oxygen and nitrogen. **Figure 5.12b** describes the shape index graph, where mapping ranges from -1Å concave to convex for the adduct. This denotes the electron density between the compounds. The red region indicates the concave, while the blue produces the convex region. The curved surface is examined in **Figure 5.12c,** in which several green flat areas are enclosed by blue edges, which correspond to the low value of the curvedness. Fragment patches represent the different color patches means that all the coordinating atoms lie in the same environment (**Figure 5.12d)**.

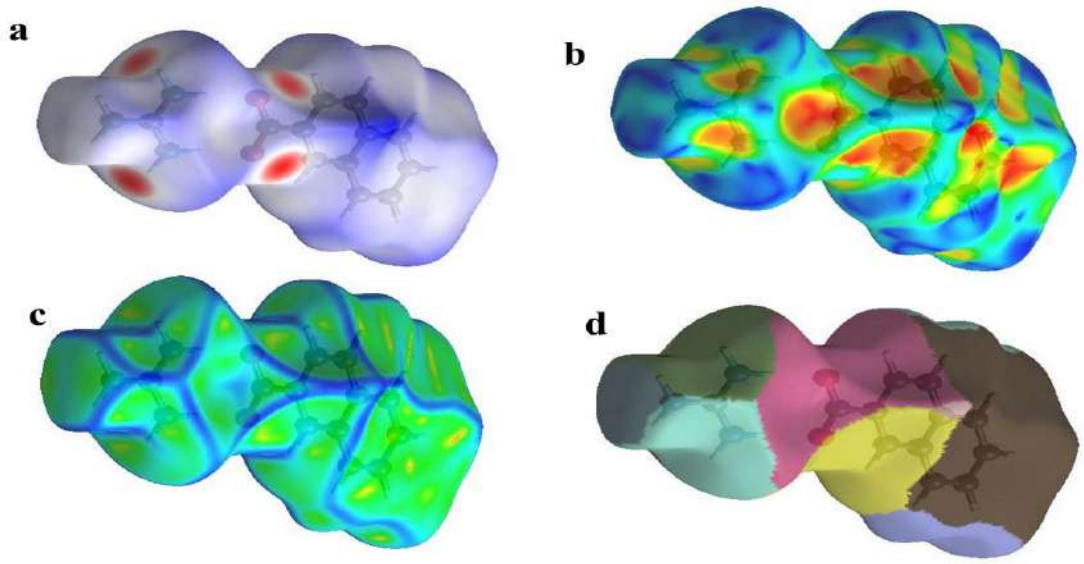

Figure 5.12 *Hirshfeld surface plots of the Acid adduct (a) d_{norm}, (b) shape index, (c) curvedness, and (d) fragment patch.*

The 2D fingerprint diagram represents the specific atomic relations and overall interactions shown in **Figure 5.13,** which represents crystal pack of H…C- 10%, C...H-18.2%, C…C-2.2%, H…H47.4% and H…O-7.0%, H…N-2.9%, N…H-3.9 %, O…C-0.2%, and C…O-0.3% other interactions is weak.

The Hirshfeld surface in **Figure 5.14a** signifies the interaction of an element inside an acid adduct with their neighborhood vicinity in the crystal package, O-overall interaction-8.0%, N- overall interaction -3.9%, H- overall interaction -67.3%, C- overall interaction -20.8%. and **Figure 5.14b** denotes the interaction of all the neighborhood atoms of the acid adduct O- overall interaction -7.3%, N- overall interaction -2.9%, H- overall interaction -77.3%, C- overall interaction -12.5%. The crystal packing for H- overall interaction shows their total interaction in the compound.

Figure 5.15 displays the voids through the unit cell axis, which determines the mechanical strength of the adduct. The volume is 187.60 $Å^3$ and the Area is 484.27 $Å^2$ [15,16,17].

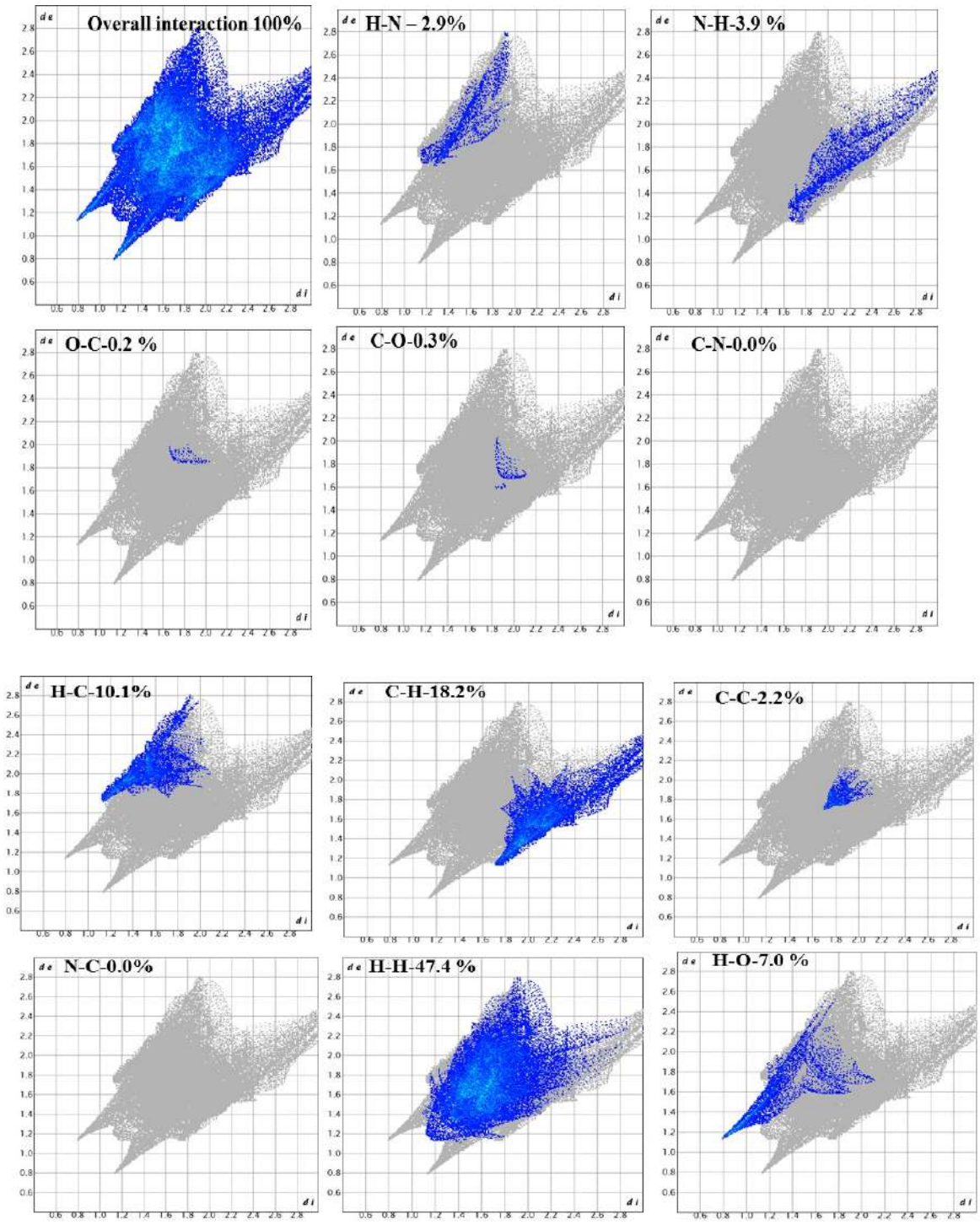

Figure 5.13 *2D fingerprints represent individual atomic interactions with overall interactions.*

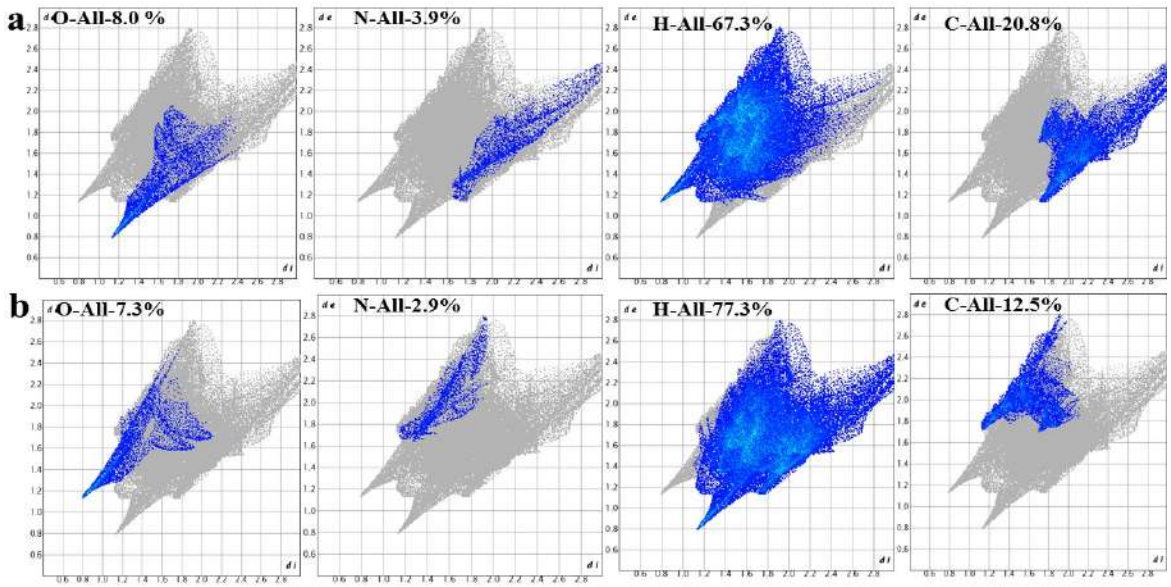

Figure 5.14 *Hirshfeld surface 2D fingerprint plots of (a) interactions of an atom inside with neighborhood vicinity atoms and (b) interactions of all the neighborhood atoms with individual elements in the crystal packing.*

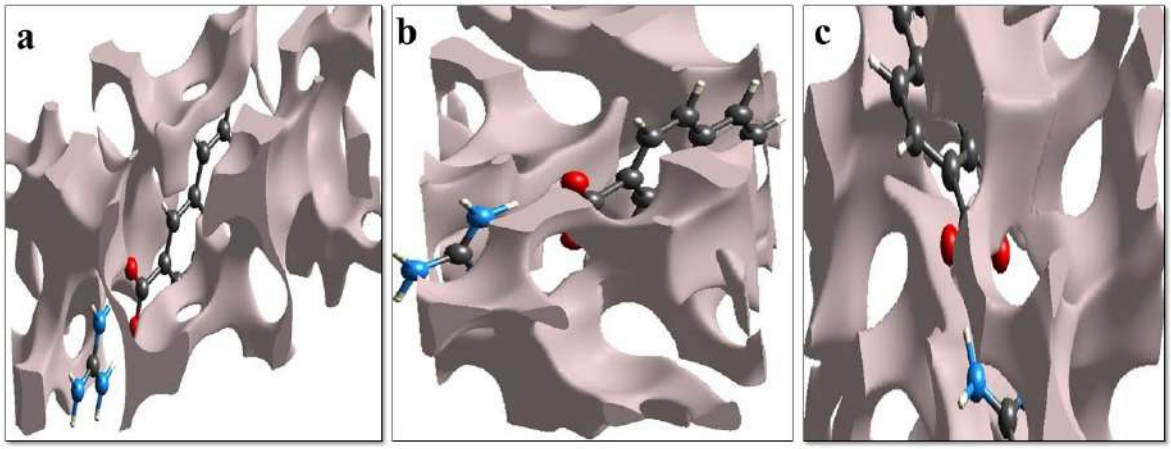

Figure 5.15 *Crystal voids of acid adduct along the a, b, and c axis.*

5.6 CONCLUSION

From the work, it was concluded that the guanidine systems form the new adducts with 2-naphthoic acid in a single crystal. The crystal system is monoclinic, and it has P_121/c 1 symmetry. Theoretical crystal morphology exhibits the eight sets of facets that are (0,0,1), (0,0,-1), (0,1,0), (0,-1,0), (1,0,0) (-1,0,0), (1,0,-1) and (-1,0,1) and the distance between the planes is found to be 13.75° angle. In IR spectra, the region around 3195- 3300 cm^{-1} is due

to the presence of N-H frequencies. The carbonyl stretching frequency was seen around 1679 cm^{-1} to 1671 cm^{-1}. The optical properties of the adduct were illustrated in the UV-visible spectroscopy, in which fundamental absorption was noticed at 4.7 e V. From Tauc's plot, the energy band gap was determined, and the value of the 4.6 eV which confirms the semi-conducting nature of the compounds. The higher refractive indexes were detected at 234 nm and lower wavelengths due to fundamental absorption. The extinction coefficient increases, after 200 nm they are gradually reduced and the skin depth of the sample, is indicated by increasing the photon energy by decreasing the skin depth value. XRD data confirms the synthesized adduct is highly crystalline. In the thermal analysis, the stability of the crystal was confirmed and the thermodynamic parameters were determined at 543K, 793K, and 953 K. The negative value of ΔS represents that the reaction is slower, the positive ΔH specifies the endothermic nature of the reaction, and the positive ΔG value proves they are non-spontaneous. The acid, base, and adduct slope values were correlated with the linear fit in which the R^2 value produced 0.99. Density function theory and frontier molecular orbital are used to estimate the possible reactivity tendency. Hirshfeld surface analysis was used to confirm the contributions of the dissimilar intermolecular interactions in the development of crystal packing.

REFERENCES

1. Aakeroy, C. B., Fasulo, M. E. & Desper, J. Cocrystal or salt: Does it really matter. *Mol. Pharm.* **4**, 317–322 (2007).
2. Karagianni, A., Malamatari, M. & Kachrimanis, K. Pharmaceutical Cocrystals: New Solid Phase Modification Approaches for the Formulation of APIs. *Pharmaceutics* **10**, (2018).
3. Arunadevi, N., Devipriya, S. & Vairam, S. The acid adducts hydrazinium 2-hy-droxy-benzoate-2-hy-droxy-benzoic acid (1/1) and hydrazinium 3-hy-droxy-2-naphtho-ate-3-hy-droxy-2-naphthoic acid (1/1). *Acta Crystallogr. Sect. C Cryst. Struct. Commun.* **68**, o61–o64 (2012).
4. Krishna Kumar, M., Sudhahar, S., Bhagavannarayana, G. & Mohan Kumar, R. Crystal growth, spectral, structural and optical studies of π-conjugated stilbazolium crystal: 4-Bromobenzaldehyde-4′-N′-methylstilbazolium tosylate. *Spectrochim. Acta Part A Mol. Biomol. Spectrosc.* **125**, 79–89 (2014).
5. Bosshard, C. Organic Nonlinear Optical Materials. *Taylor Fr.* **1st Editio**, 256 (2020).
6. Swathika, M. & Natarajan, A. Synthesis and photometric properties of efficient white-emitting phosphor of M-AMG transition metal complexes for OLED applications. *Luminescence* (2022).
7. Ma, Y. *et al.* Growth, structural, thermal, dielectric and optical studies on HBST crystal: A potential THz emitter. *Spectrochim. Acta Part A Mol. Biomol. Spectrosc.* **190**, 274–282 (2018).
8. Rai, R. N. *et al.* Crystal growth and nonlinear optical studies of m-dinitrobenzene doped urea. *J. Cryst. Growth* **321**, 72–77 (2011).
9. Priyadarshini, P. *et al.* Observation of high nonlinearity in Bi doped BixIn35-xSe65 thin films with annealing. *Sci. Reports 2021 111* **11**, 1–13 (2021).
10. Donia, A. M. & Ayad, M. I. Thermal behaviour of some crystal solvates of magnanese(III) complexes. *Monatshefte für Chemie / Chem. Mon. 1993 12410* **124**, 981–986 (1993).

11. Arunadevi, N. *et al.* Synthesis and crystal growth of cadmium naphthoate crystal for second order non-linear optics and cytotoxic activity. *J. Dispers. Sci. Technol.* **43**, 2192–2208 (2022).

12. Hamada, M. M., Shallaby, A. H. M., El-Shafai, O. & El-Asmy, A. A. Spectroscopic Characterization and Catalytic Activity of Some Cu(II)-thiosemicarbazide Complexes. *Transit. Met. Chem.* **31**, 522–529 (2006).

13. Ashfaq, M. *et al.* Single crystal investigation, Hirshfeld surface analysis and DFT exploration of the pyrimethamine-based novel organic salt: 2, 4-diamino-5-(4-chlorophenyl)-6-ethylpyrimidin-1-ium 3-carboxybenzoate hydrate (1:1:1). *J. Mol. Struct.* **1224**, 129309 (2021).

14. Gatfaoui, S. *et al.* Synthesis, structural and spectroscopic features, and investigation of bioactive nature of a novel organic-inorganic hybrid material 1H-1,2,4-triazole-4-ium trioxonitrate. *J. Mol. Struct.* **1150**, 242–257 (2017).

15. Venkateshan, M., Priya, R. V., Muthu, M., Suresh, J. & Kumar, R. R. Crystal structure, Hirshfeld surface analysis, DFT calculations and molecular docking studies on pyridine derivatives as potential inhibitors of NAMPT. *Chem. Data Collect.* **23**, 100262 (2019).

16. Al-Resayes, S. I. *et al.* Structural and theoretical investigations, Hirshfeld surface analyses, and cytotoxicity of a naphthalene-based chiral compound. *ACS Omega* **5**, 27227–27234 (2020).

17. Turner, M. J., McKinnon, J. J., Jayatilaka, D. & Spackman, M. A. Visualisation and characterisation of voids in crystalline materials. *CrystEngComm* **13**, 1804–1813 (2011).